ISSN 2176-5480

22nd International Congress of Mechanical Engineering (COBEM 2013)
November 3-7, 2013, Ribeirão Preto, SP, Brazil

DISCONTINUITY INDUCED BIFURCATION IN AEROELASTIC SYSTEMS WITH FREEPLAY NONLINEARITY

Rui Vasconcellos
São Paulo State University, São João da Boa Vista-SP, Brazil
rui.vasconcellos@sjbv.unesp.br
Abdessattar Abdelkefi
Muhammad R. Hajj
Department of Engineering Science and Mechanics, MC 0219, Virginia Polytechnic Institute and State University, Blacksburg, Virginia 24061, USA.
abdes09@vt.edu
Flávio Marques
Laboratory of Aeroelasticity, Universty of São Paulo, Brazil
fmarques@sc.usp.br

Abstract. *A nonlinear analysis is performed to determine the effects of a nonsmooth function on the behavior of an aeroelastic system and its relation to the grazing bifurcation and period-doubling responses. This system consists of a plunging and pitching rigid airfoil supported by linear spring in the plunge degree of freedom and a nonlinear spring in the pitch degree of freedom. The nonsmooth function is presented by the freeplay nonlinearity in the pitch degree of freedom of an aeroelatic system. This freeplay nonlinearity is modeled based on a hyperbolic tangent representation. The aerodynamic loads are modeled based on the unsteady formulation. A linear analysis is performed to determine the coupled damping and frequencies and the associated linear flutter speed. Then, a nonlinear analysis is performed to determine the effects of the freeplay size on the behavior of the aeroelastic system. To this end, two different pitch freeplay gaps are considered. The results show that, for both considered freeplay gaps, there are two different transitions or sudden jumps are observed when varying the freestream velocity (below linear flutter speed). It is demonstrated that these sudden transitions are due to the fact of the tangential contact between the trajectory and the freeplay boundaries (grazing bifurcation). The results also show that near these transitions the pitch motion changes response from periodic to period-doubling in the first transition and from period-doubling to periodic in the second transition.*

Keywords: *Grazing bifurcation, Aeroelasticity, Freeplay nonlinearity, Period-doubling, Nonlinear dynamics.*

INTRODUCTION

Concentrated nonlinearities, such as the cubic stiffness and the freeplay are commonly found in an aeroelastic system. The freeplay nonlinearity exists in control surface attachments of different flight vehicles which is due to loosened mechanical linkages and manufacturing tolerances. The presence of freeplay nonlinearity in an aeroelastic system may lead to complex and undesirable responses, such as instabilities, limit cycle oscillations (LCO), chaos and abrupt transitions due to bifurcation. The presence of these undesirable behaviors oblige researchers to investigate and evaluate freeplay nonlinearity effects during the vehicle flight. Virgin *et al.* Virgin *et al.* (1999), Conner *et al.* Conner *et al.* (1996), Trickey *et al.* Trickey *et al.* (2002), and Vasconcellos *et al.* Vasconcellos *et al.* (2012) have studied numerically and experimentally the effects of a freeplay nonlinearity in the flap degree of freedom on the behavior of an aeroelastic system. They showed that different transitions can occur, such as from damped to periodic LCOs to quasi-periodic responses, and then, to chaotic motions. These transitions were observed at airspeeds lower than the linear flutter speed Conner *et al.* (1996); Fung (1993); Abdelkefi *et al.* (2012a,b).

Grazing bifurcations of limit cycles are one of the most commonly found discontinuity-induced bifurcations (DIBs) di Bernardo *et al.* (2006). These types of bifurcations are caused by a limit cycle that becomes tangent to the discontinuity boundary of the available piecewise-smooth function. These types of bifurcations can occur only to piecewise smooth systems. Piecewise smooth systems can be found in various systems or impact oscillators, such as shock sensors, gears, cutting tools, tapping mode atomic force microscopy, and aeroelastic systems with freeplays. Many researchers studied different elastic structures undergoing impacts Moon and Shaw (1983); Shaw and Holmes (1983); Shaw (1985); Whiston (1987); Nordmark (1991); Chin *et al.* (1994). A special phenomenon arises during zero-speed incidence which is refereed to "grazing impacts", this phenomenon is originally showed by Whiston Whiston (1987). Grazing bifurcations have been studied by several researchers in elastic structure, such as spring-mass system Shaw and Holmes (1983); Nordmark (1991); Stensson and Nordmark (1994); Chin *et al.* (1994); Virgin and Begley (1999); Molenaar *et al.* (2001); Dankowicz *et al.* (2007), cantilever beams Moon and Shaw (1983); Shaw (1985); de Weger *et al.* (1996); Long *et al.* (2008); Dick *et al.* (2009); Chakraborty and Balachandran (2012).

In their work, they investigated the effects of many parameters and excitations on the grazing bifurcation, such as

ISSN 2176-5480

Table 1: Concentrated typical section parameters of the aeroelastic wing

$span$	Wing span (m)	0.5
b	Wing semi-chord (m)	0.125
a	Position of elastic axis relative to the semi-chord	-0.5
ρ_p	Air density (kg/m^3)	1.1
m_w	Mass of the wing (kg)	1.716
m_T	Mass of wing and supports (kg)	3.53
r_α^2	radius of gyration square (kgm^2)	0.684
ω_α	natural frequency of pitch (rad/s)	80
ω_h	natural frequency of plunge (rad/s)	30
x_α	Nondimensional distance between center of gravity and elastic axis	0.6

low-speed impacts Stensson and Nordmark (1994), friction and hard impacts Chin *et al.* (1994), harmonic and aharmonic impacts Balachandran (2003), off-resonance excitations Dick *et al.* (2009). Because the freeplay nonlinearity is a nonsmooth function that generally exists in aeroelastic system, grazing bifurcation can take place and then a new feature in aeroelastic systems can happen. In this work, we investigate grazing bifurcations in a two degrees of freedom aeroelastic system with a freeplay nonlinearity in the pitch degree of freedom. This system consists of a plunging and pitching rigid airfoil supported by linear spring in the plunge degree of freedom and a nonlinear spring in the pitch degree of freedom. The governing equations of the considered aeroelastic system are described in Section 2. In Section 3, the nonsmooth function which is presented by the freeplay nonlinearity is modeled by hyperbolic tangent representation. In Section 4, the aerodynamic loads are modeled based on the unsteady formulation. Linear and nonlinear analyses are performed in Section 5. Summary and conclusions are presented in Section 6.

NONLINEAR AEROELASTIC MODEL

The aeroelastic system consists of a two-dimensional airfoil that has two degrees of freedom including pitch and plunge motions. The plunge and pitch motions are measured at the elastic axis which are denoted by h and α, respectively. The distance from the elastic axis to mid-chord is represented by ab where a is a constant and b is the semi-chord length of the entire airfoil section. The mass center of the entire airfoil is located at a distance $x_\alpha b$ from the elastic axis. The two spring forces for plunge and pitch are represented by k_h and k_α, respectively. The viscous damping forces are described through the coefficients c_h and c_α for plunge and pitch, respectively. Finally, U is used to denote the freestream velocity. Using Lagrange's equations, the equations of motion governing this system are written as:

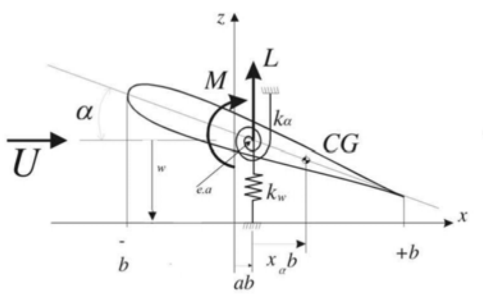

Figure 1: Schematic of an aeroelastic system under uniform airflow

$$\begin{bmatrix} m_T & m_w x_\alpha b \\ m_w x_\alpha b & I_\alpha \end{bmatrix} \begin{bmatrix} \ddot{h} \\ \ddot{\alpha} \end{bmatrix} + \begin{bmatrix} c_h & 0 \\ 0 & c_\alpha \end{bmatrix} \begin{bmatrix} \dot{h} \\ \dot{\alpha} \end{bmatrix} + \begin{bmatrix} k_h & 0 \\ 0 & k_\alpha F(\alpha)/\alpha \end{bmatrix} \begin{bmatrix} h \\ \alpha \end{bmatrix} = \begin{bmatrix} -L \\ M \end{bmatrix} \tag{1}$$

where m_T is the mass of the entire system (wing and support), m_w is the wing mass alone, I_α is the mass moment of inertia about the elastic axis. The values of these parameters used in the following analysis are given in Table 1. In addition, L and M are the aerodynamic lift and moment about the elastic axis. $F(\alpha)$ is a function used to represent the pitch freeplay nonlinearity in the system.

The function is known by its discontinuous representation to account for the freeplay effect, $F(\alpha)$ is given by:

$$F(\alpha) = \begin{cases} \alpha + \delta \ , & \text{if } \alpha < -\delta \ , \\ 0 \ , & \text{if } \mid \alpha \mid \leq \delta \ , \\ \alpha - \delta \ , & \text{if } \alpha > \delta \ . \end{cases} \tag{2}$$

ISSN 2176-5480

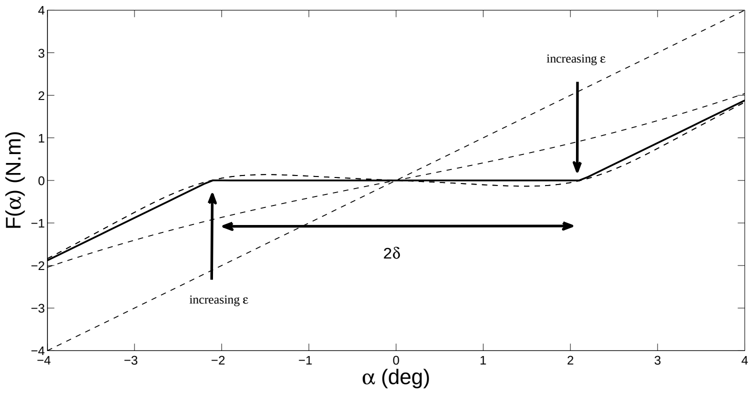

Figure 2: Pitch angle *versus* torque described in Eq. (3), ε increasing from 0 to 100

Using this discontinuous function, different methods can be used to solve the governing equations, such as Henon's method Henon (1982). These methods require multiple time-integrations and they are time consuming Jones *et al.* (2007); Roberts *et al.* (2002). To solve this issue, Vasconcellos et al. Vasconcellos *et al.* (2012) used the tangent hyperbolic representation (continuous function) to model this discontinuous function. They reported that this representation can be used effectively to model the freeplay nonlinearity. The mathematical formulation for this representation is given by:

$$F(\alpha) = \frac{1}{2}\left[1-\tanh(\varepsilon(\alpha+\delta))\right]\,(\alpha+\delta)+\frac{1}{2}\left[1+\tanh(\varepsilon(\alpha-\delta))\right]\,(\alpha-\delta) \tag{3}$$

where δ denotes freeplay boundary region, and ε is a variable which affects the smoothness of the function, thereby determining the accuracy of the approximation. In Eq.(3), as ε value increases, the hyperbolic tangent functions combination becomes more representative of the real freeplay effect. This feature is shown in Figure 2 as obtained by using Eq. (3) for $\delta = 2.12°$, and for various values of ε. Clearly, as ε goes to infinity, the representation for $F(\alpha)$ leads to the real freeplay discontinuous effect.

1. REPRESENTATION OF AERODYNAMIC LOADS

The aerodynamic loads are modeled using Theodorsen approach Theodorsen (1935), where the unsteady aerodynamic forces and moments are written respectively as:

$$L = \pi\rho b^2\left[\ddot{h}+U\dot{\alpha}-ba\ddot{\alpha}\right]+2\pi\rho UbQC \tag{4}$$

and

$$M_\alpha = \pi\rho b^2\left[ba\ddot{h}-Ub\left(\frac{1}{2}-a\right)\dot{\alpha}-b^2\left(\frac{1}{8}+a^2\right)\ddot{\alpha}\right]+2\pi\rho b^2U(a+\frac{1}{2})QC \tag{5}$$

where U is the freesteram velocity, C is the Theodorsen function, and

$$Q = U\alpha+\dot{h}+\dot{\alpha}b\left(\frac{1}{2}-a\right) \tag{6}$$

The aerodynamic loads given in Eqs. (4) and (5) depend on Theodorsen function $C(k)$, where $k = \frac{\omega b}{U}$ is the reduced frequency of harmonic oscillations. Considering the unsteady effect in the flow, the aerodynamic loads associated with Theodorsen function can be manipulated by convolution based on Duhamel formulation in the time domain Edwards *et al.* (1979); Bisplinghoff *et al.* (1996); Abdelkefi *et al.* (2012b). Using the Sears and Pade approximations, the unsteady representation of the aerodynamic loads are modeled as follows Abdelkefi *et al.* (2012b):

$$L = \pi\rho b^2\left[\ddot{h}+U\dot{\alpha}-ba\ddot{\alpha}\right]+2\pi\rho Ub(c_0-c_1-c_3)Q+\qquad 2\pi\rho U^3c_2c_4(c_1+c_3)\bar{x}+2\pi\rho U^2b(c_1c_2+c_3c_4)\dot{\bar{x}} \tag{7}$$

and

$$\begin{aligned}M_\alpha = \pi\rho b^2&\left[ba\ddot{h}-Ub\left(\frac{1}{2}-a\right)\dot{\alpha}-b^2\left(\frac{1}{8}+a^2\right)\ddot{\alpha}\right]+2\pi\rho b^2U(a+\frac{1}{2})(c_0-c_1-c_3)Q\\ &+2\pi\rho bU^3(a+\frac{1}{2})c_2c_4(c_1+c_3)\bar{x}+2\pi\rho b^2U^2(a+\frac{1}{2})(c_1c_2+c_3c_4)\dot{\bar{x}}\end{aligned} \tag{8}$$

where $c_0 = 1$, $c_1 = 0.165$, $c_2 = 0.0455$, $c_3 = 0.335$, and $c_4 = 0.3$. These coefficients are present due to the Sears approximation to the Wagner function. $\bar{x}$ and $\dot{\bar{x}}$ are two augmented variables in the state space. They are related to the system variables by the following second-order differential equation:

$$\ddot{\bar{x}} = -c_2c_4\frac{U^2}{b^2}\bar{x}-(c_2+c_4)\frac{U}{b}\dot{\bar{x}}+\frac{U}{b}\alpha+(\frac{1}{2}-a)\dot{\alpha}+\frac{\dot{h}}{b} \tag{9}$$

More details for the derivation of the aerodynamic loads based on the Duhamel formulation can be found in Abdelkefi et al. Abdelkefi *et al.* (2012b).

NONLINEAR ANALYSIS: GRAZING BIFURCATION

To investigate the effects of the freeplay nonlinearity on the behavior of the aeroelastic system, we perform a nonlinear analysis. To this end, the freeplay nonlinearity which is modeled by Eq. 3 is introduced in the governing equations. Two different freeplay gap values are considered which are respectively $\delta = 0.1deg$ and $\delta = 0.5deg$.

First freeplay gap ($\delta = 0.1deg$)

For the first configuration when $\delta = 0.1deg$, we consider the following initial conditions ($h(0) = 0.001m, \alpha(0) = 0.1deg., \alpha'(0) = 0, h'(0) = 0$). It is noted that the wing oscillates for a range of freestream velocity below the linear flutter speed. Consequently, the numerical simulations are carried out for freestream velocities starting from $9.5m/s$, when the wing presents self-sustained motions. Then, the freestream velocity is increased by steps of $0.1m/s$ after 6 seconds of motion, until reach the speed of $40m/s$.

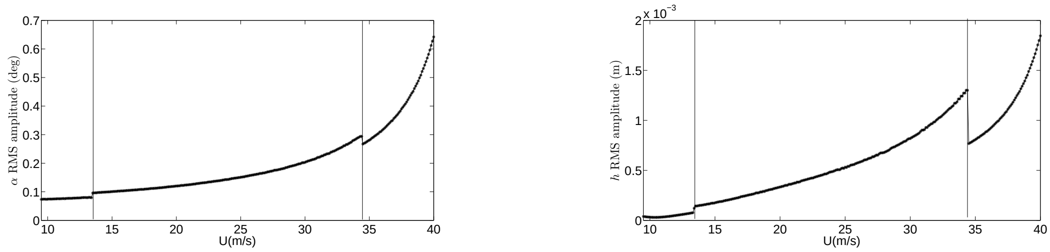

(a) (b)

Figure 3: Variations of (a) RMS pitch amplitude and (b) RMS plunge amplitude when increasing the freestream velocity.

The plotted curves in Figure 3 show the variations of the RMS values of the pitch and plunge motions as a function of the freestream velocity. It follows from these plots that there are three different regions. The first one is observed when the freestream velocity is between $9.5m/s$ and $13.4m/s$. In this region, it is noted that increasing the freestream velocity is accompanied by an increase in the pitch and plunge RMS amplitudes. When $U = 13.4m/s$, a small-sudden jump in both motions is obtained with an increase in the RMS values of the pitch and plunge motions. The second region is observed when the freestream velocity varies from $13.4m/s$ and $34.4m/s$. When the freestream velocity is increased, the RMS values of both the pitch and plunge motions are increased. When $U = 34.4m/s$, another sudden which results in a decrease in the RMS values of the pitch and plunge motions. However, this jump is more significant in the plunge motion, as shown in Figure 3(b). The third region is obtained when the freestream velocity is increased from $34.4m/s$ to $40m/s$. In this region, the RMS pitch and plunge amplitudes restart increasing when the freestream velocity is increased. Therefore, two different transitions are obtained when varying the freestream velocity. The first one when $U = 13.4m/s$ and the second one when $U = 34.4m/s$. To determine the reasons behind these two transitions, we focus next near these transitions with performing a time series analyses.

First transition

For the first transition which is observed at $U = 13.4m/s$, we plot in Figures 4 the time histories of the pitch and plunge motions for two different freestream velocities which are considered just directly before and after this transition. Inspecting these plots, we note the appearance of new harmonics in the pitch motion. Furthermore, the amplitudes of both motions are increased when the freestream velocity is considered after the transition. The appearance of more frequencies after the transition in the pitch motion is explained in its correspondent power spectrum, as shown in Figure 5(b). Inspecting the power spectra of both the pitch and plunge motions, as presented in Figure 5, we note that when the freestream velocity is larger than $13.4m/s$, there are new frequencies are appeared and some other frequencies are disappeared. At this speed, there are two dominant frequencies. The second frequency is more important in the pitch motion than in the plunge motion, as shown in Figures 5(b) and (d), respectively.

The plotted curves in Figure 6 show the phase portraits for different freestream velocities before and after the first transition. For the plunge motion, it is noted that the system almost behave the same. As predicted, there is a transition in the pitch degree of freedom from periodic motion to period-doubling motion. The discontinuity in this freeplay case occurs when the pitch angle is equal to $0.1deg$ (half-size of the considered freeplay). Inspecting the phase portrait of the pitch motion which is plotted in Figure 6(b), the period-doubling event happens near the freeplay discontinuity ($\pm 0.1deg$) . Consequently, this first transition is associated with a near grazing bifurcation.

ISSN 2176-5480

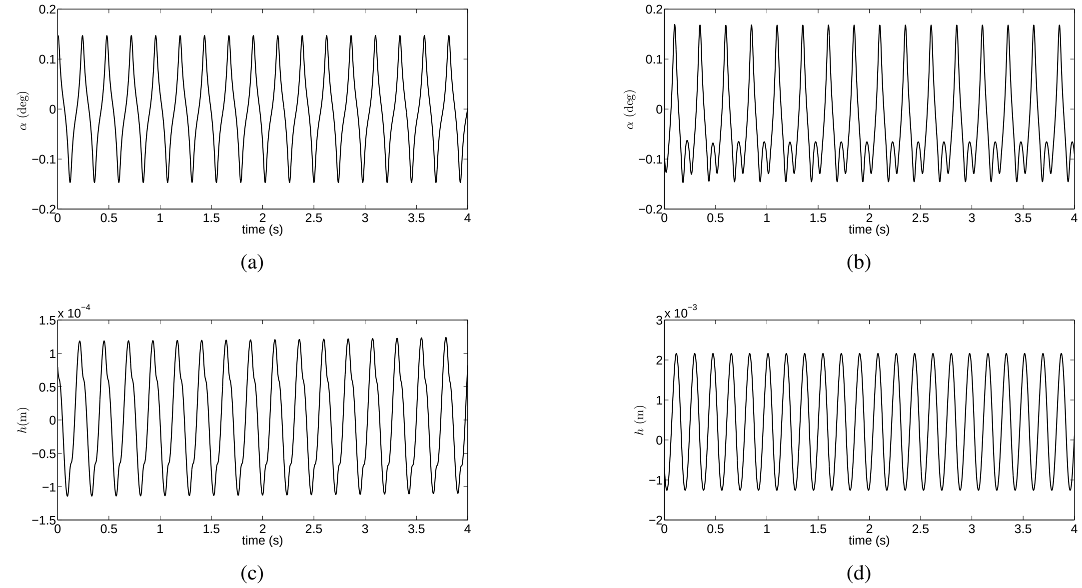

Figure 4: Time series of the pitch and plunge motions (a,c) before the first transition ($13.3m/s$) and (b,d) after the first transition ($13.5m/s$).

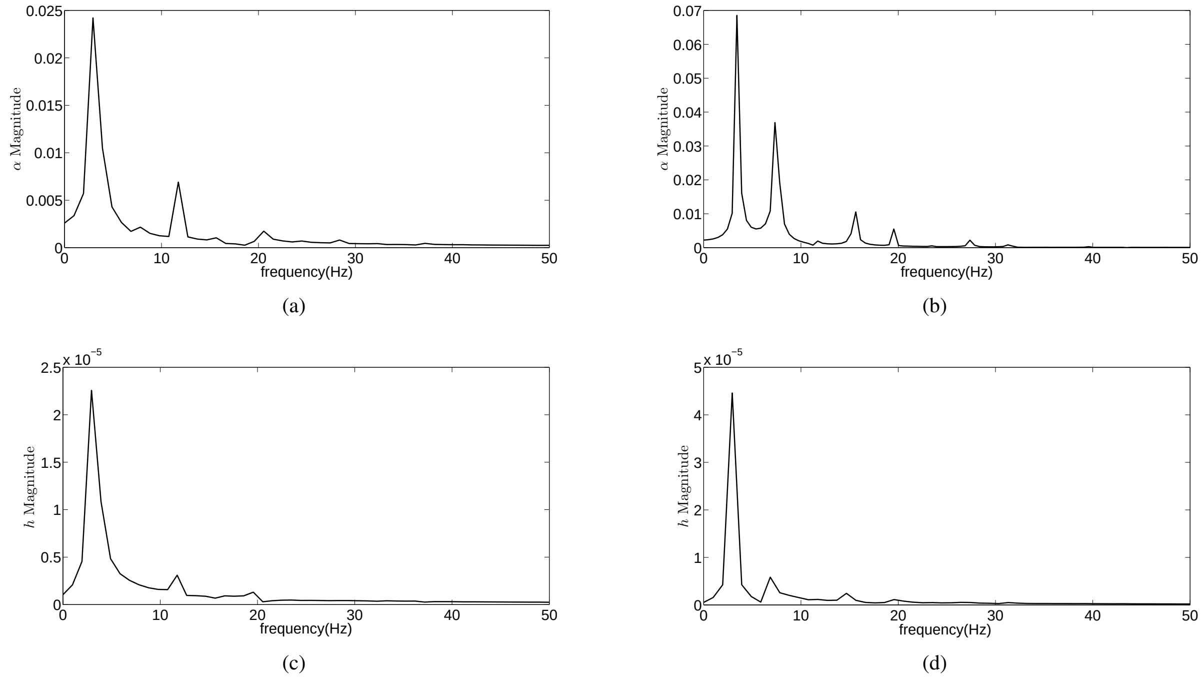

Figure 5: Power spectra of the pitch and plunge motions (a,c) before the first transition ($13.3m/s$) and (b,d) after the first transition ($13.5m/s$).

Second transition

We investigate the behavior of the aeroelastic system near the second transition or jump. To this end, we perform the same time series analyses as used to study the first transition. In Figures 7 and 9, the time histories and power spectra of the pitch and plunge motions are plotted for two different freestream velocities smaller and larger than $34.4m/s$. Clearly, it is noted that the aeroelastic system changes behavior. In fact, the response of the pitch motion is changed from period-doubling for freestream velocity smaller than $34.4m/s$ to periodic response for freestream velocity larger than $34.4m/s$. Concerning the plunge motion, the response is periodic for both considered freestream velocity. This is predicted due to the fact that the freeplay discontinuity is associated to the pitch degree of freedom. The change in the pitch motion before and after the transition is probably due to grazing bifurcation. To investigate this transition form period-doubling to periodic responses and its possible relation to grazing bifurcations, we plot in Figure 9 the phase portraits of the pitch and plunge motions for both considered freestream velocities. It is noted that there is a small loop in Figure 9(b) which

ISSN 2176-5480

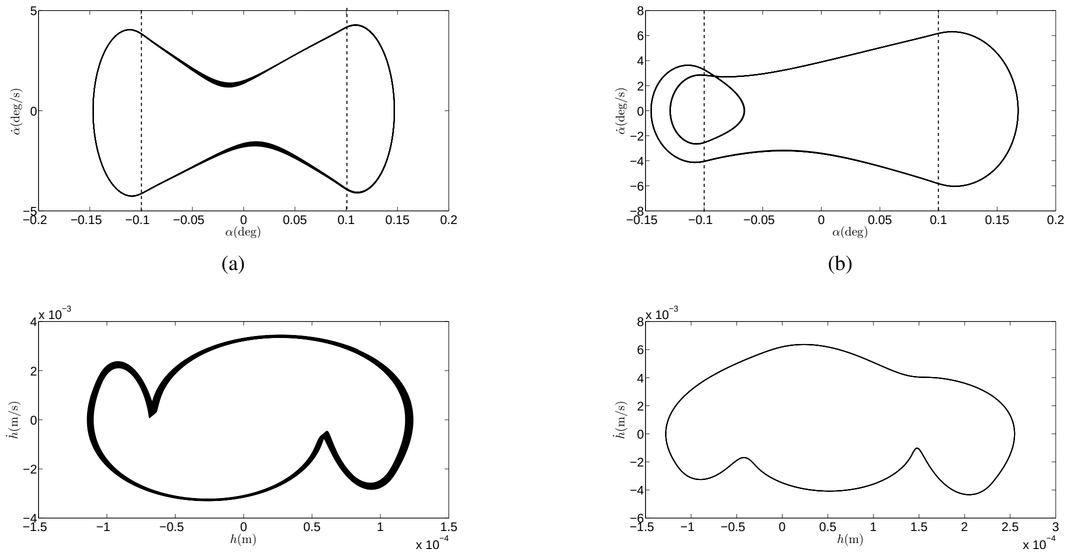

(a) (b)

(c) (d)

Figure 6: Phase portrait of the pitch and plunge motions (a,c) before the first transition ($13.3m/s$) and (b,d) after the first transition ($13.5m/s$).

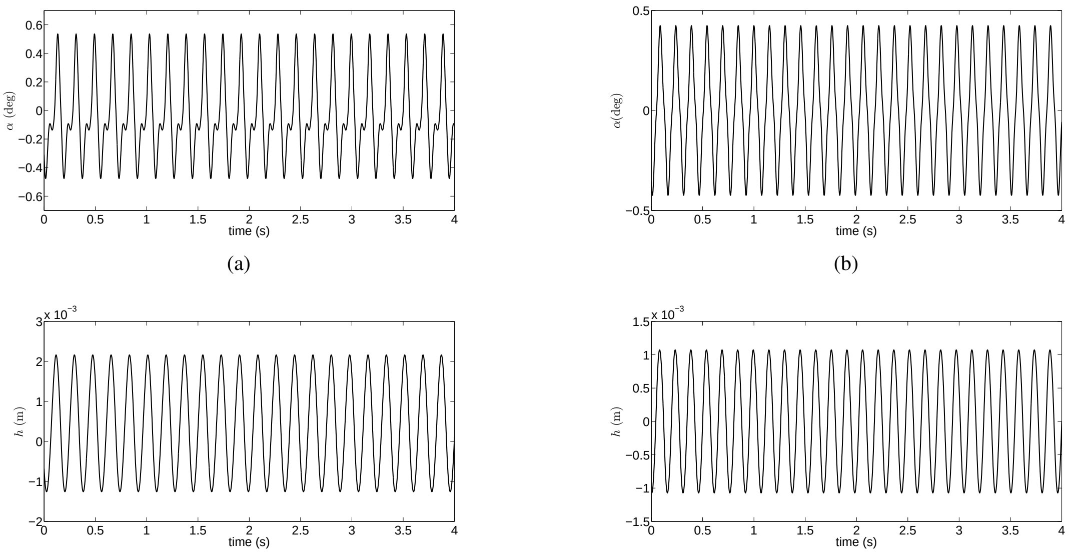

(a) (b)

(c) (d)

Figure 7: Time histories of the pitch and plunge motions (a,c) before the second transition ($34.3m/s$) and (b,d) after the second transition ($34.5m/s$).

is tangent to the freeplay discontinuity boundary and with a zero-pitch speed incidence. This is exactly the definition of a grazing bifurcation. Consequently, the appearance and disappearance of the period-doubling responses are associated to the near grazing and grazing bifurcations and which is also associated with two sudden jumps or transitions.

Second freeplay gap ($\delta = 0.5deg$)

In order to confirm the occurrence of grazing bifurcation in aeroelastic systems with freeplay nonlinearity, we consider a second freeplay gap or discontinuity. The freeplay gap is considered equal to $0.5deg$ and the rest of the parameters are considered the same as the first case of freeplay gap. For the second configuration when $\delta = 0.5deg$, we consider the following initial conditions ($h(0) = 0.001m, \alpha(0) = 0.5deg, \alpha'(0) = 0, h'(0) = 0$). Same as the first configuration of freeplay gap, the wing oscillates for a range of freestream velocity below the linear flutter speed. Therefore, the numerical simulations are carried out for freestream velocities starting from $9.5m/s$ until reaches a freestream velocity of $40m/s$.

Figures 10(a) and (b) show the variations of the RMS values of the pitch and plunge motions when increasing the freestream velocity. Similar to the first configuration of freeplay gap, three different regions are observed. The first one is observed when the freestream velocity is between $9.5m/s$ and $13.4m/s$ which is the same region of the first configuration

ISSN 2176-5480

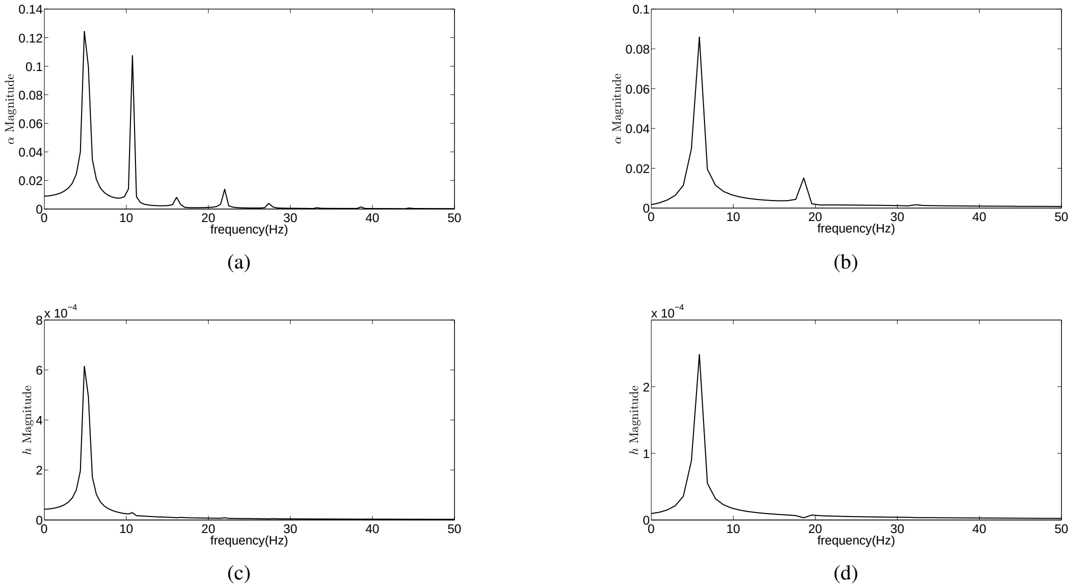

Figure 8: Power spectra of the pitch and plunge motions (a,c) before the second transition ($34.3m/s$) and (b,d) after the second transition ($34.5m/s$).

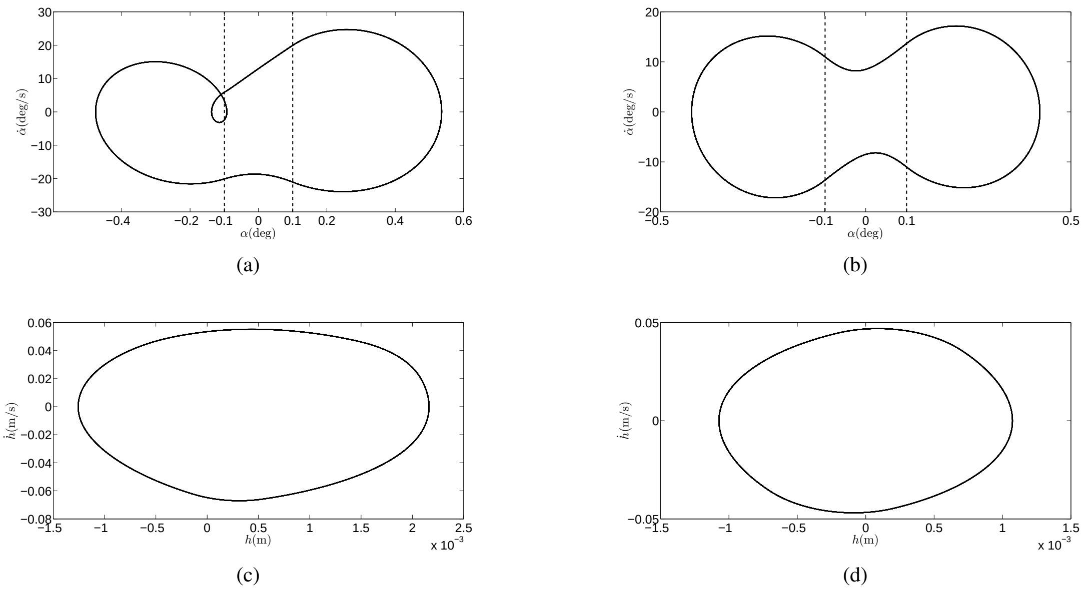

Figure 9: Phase portrait of the pitch and plunge motions (a,c) before the second transition ($34.3m/s$) and (b,d) after the second transition ($34.5m/s$).

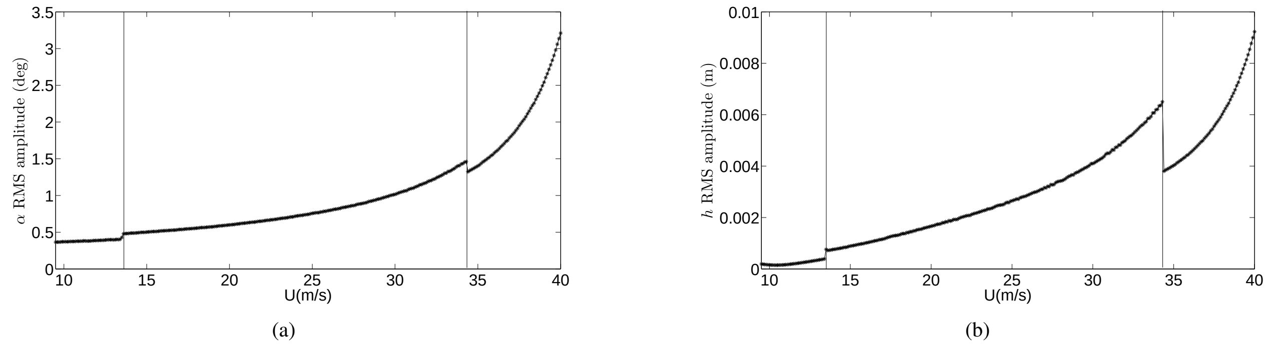

Figure 10: Variations of (a) RMS pitch amplitude and (b) RMS plunge amplitude when increasing the freestream velocity.

of freeplay gap. We note that the freeplay size does not change the first transition freestream velocity. The second region

ISSN 2176-5480

is observed when the freestream velocity varies from $13.4m/s$ and $34.3m/s$. At $U = 34.3m/s$, the second transition takes place with a decrease in the RMS values of the pitch and plunge motions. Compared to the first configuration of freeplay gap, there is a small decrease in the freestream velocity of the second configuration of freeplay. The third region is obtained when the freestream velocity is increased from $34.3m/s$ to $40m/s$. The same investigation is performed in the rest of this section in order to determine if these jumps are associated with a near grazing or grazing bifurcations. To this end, we focus near these transitions with performing a time series analyses, as discussed in the previous sections.

First transition

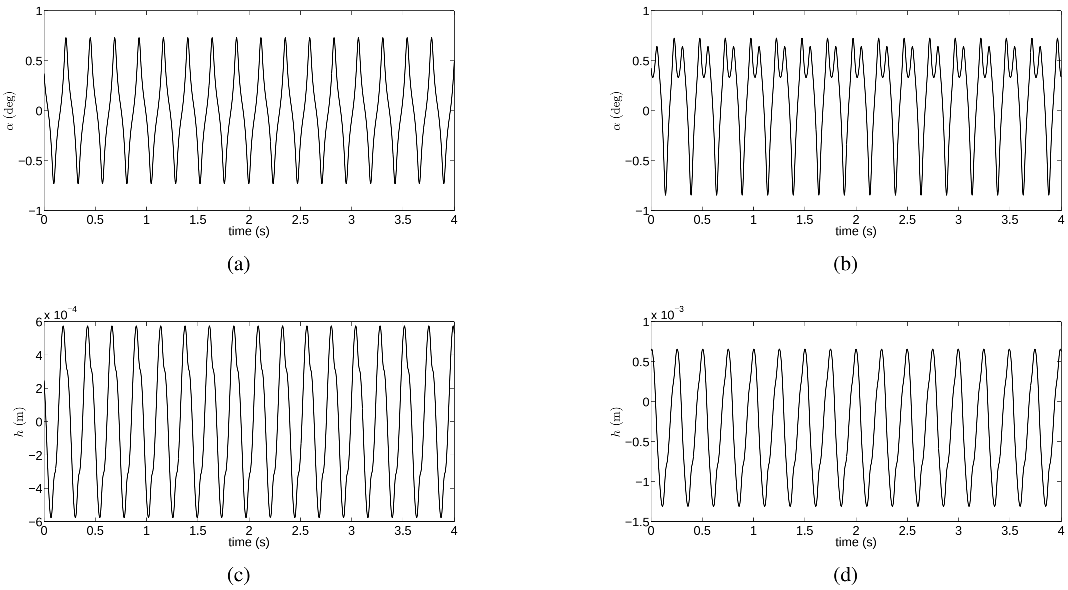

Figure 11: Time histories of the pitch and plunge motions (a,c) before the first transition ($13.3m/s$) and (b,d) after the first transition ($13.5m/s$).

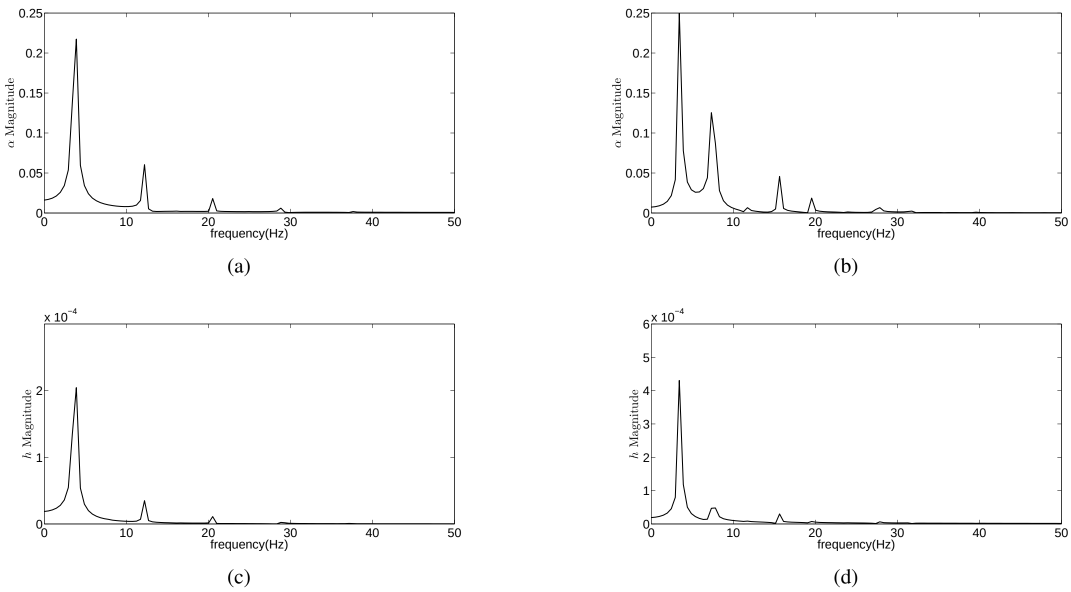

Figure 12: Power spectrum of the pitch and plunge motions (a,c) before the first transition ($13.3m/s$) and (b,d) after the first transition ($13.5m/s$).

To determine the behavior of the aeroelastic system and the associated jump or transition when $U = 13.4m/s$, we plot in Figures 11 and 12 the time histories and power spectra of the pitch and plunge motions for two different freestream velocities which are considered just directly before and after this transition. It follows from these figures that there is appearance of new harmonics or period-doubling in the pitch motion when the freestream velocity is larger than $13.4m/s$ compared to periodic response when the freestream velocity is smaller than $13.4m/s$. On the other hand, the plunge motion is periodic for both considered speed. To determine the cause of this change in the pitch motion, we plot in

ISSN 2176-5480

Figure 13 the phase portraits of both the pitch and plunge motions. It is noted that when the freestream velocity is larger than $13.4m/s$ there is a small loop which intersects the freeplay boundary ($\delta = 0.5deg$) and also intersects the zero-pitch speed. Consequently, a near grazing impacts is occurred in this transition or jump.

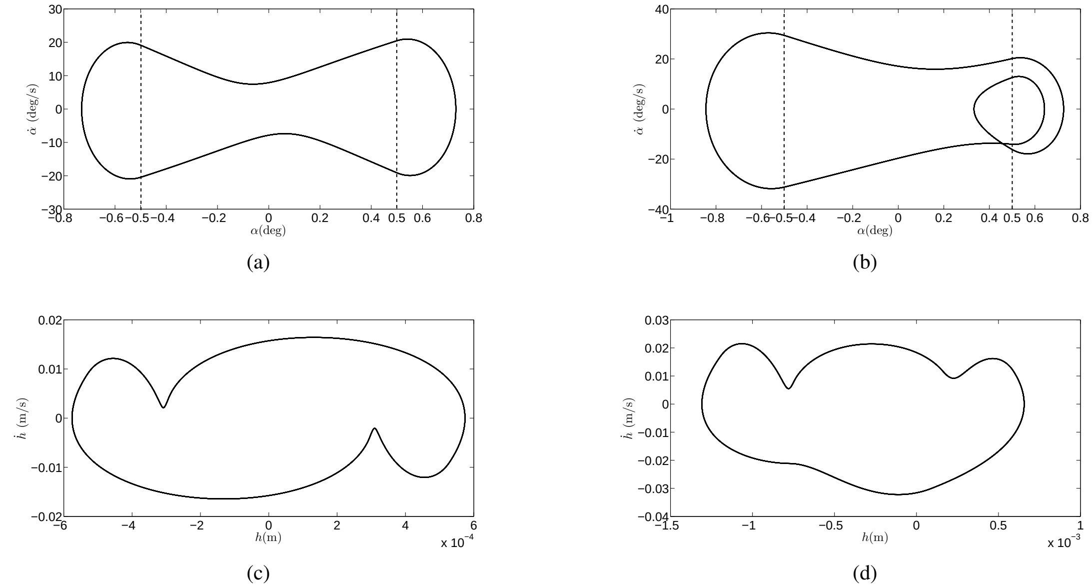

Figure 13: Phase portrait of the pitch and plunge motions (a,c) before the first transition ($13.3m/s$) and (b,d) after the first transition ($13.5m/s$).

1.0.1 Second transition

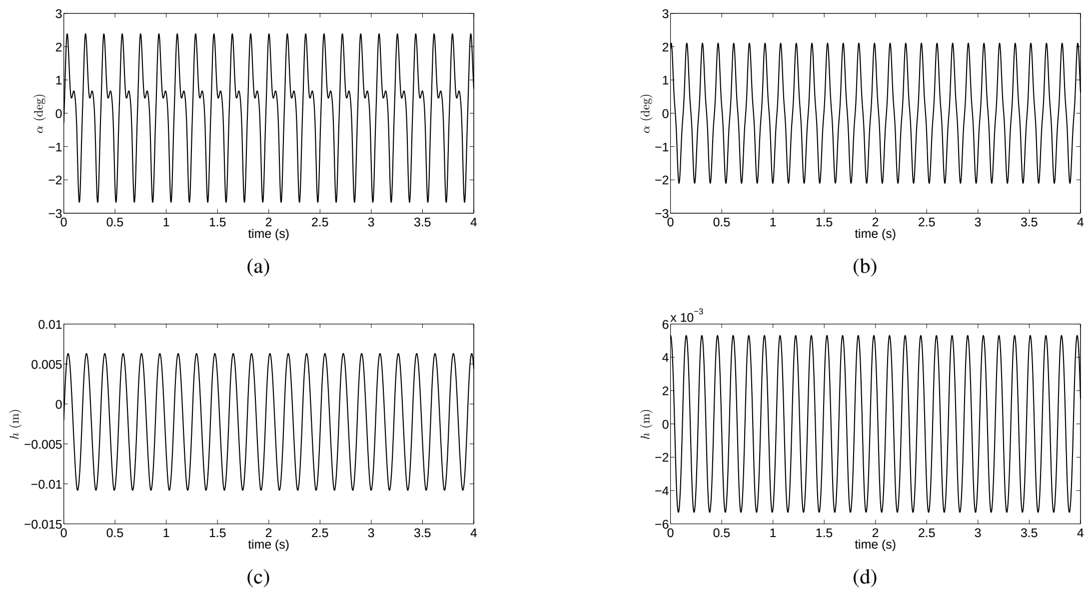

Figure 14: Time histories of the pitch and plunge motions (a,c) before the second transition ($34,2m/s$) and (b,d) after the second transition ($34,4m/s$).

In this section, the behavior of the considered aeroelastic system near the second transition is investigated. Same time series analyses are performed in terms of time histories, power spectra and phase portraits. The plotted curves in Figures 14 and 16 show the time histories and power spectra of the pitch and plunge motions for two different freestream velocities smaller and larger than $34.3m/s$. Inspecting these figures, we note that the response of the pitch motion is changed from period-doubling response to periodic response when the freestream velocity is increased near $34.3m/s$. As the other transitions, the plunge response is always periodic for both considered freestream velocity. The cause of this transition from period-doubling to periodic responses is explained when plotting the phase portrait plots for freestream velocities are smaller and larger than $34.3m/s$, as shown in Figures 16(a)(a) and (b). A small loop is observed tangent to

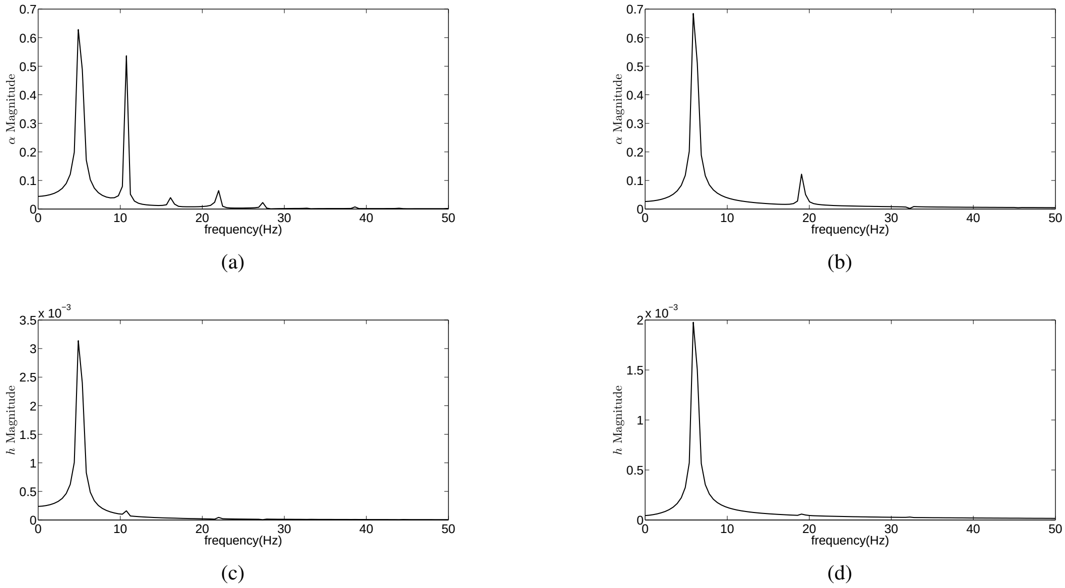

Figure 15: Power spectra of the pitch and plunge motions (a,c) before the second transition $(34, 2m/s)$ and (b,d) after the second transition $(34, 4m/s)$.

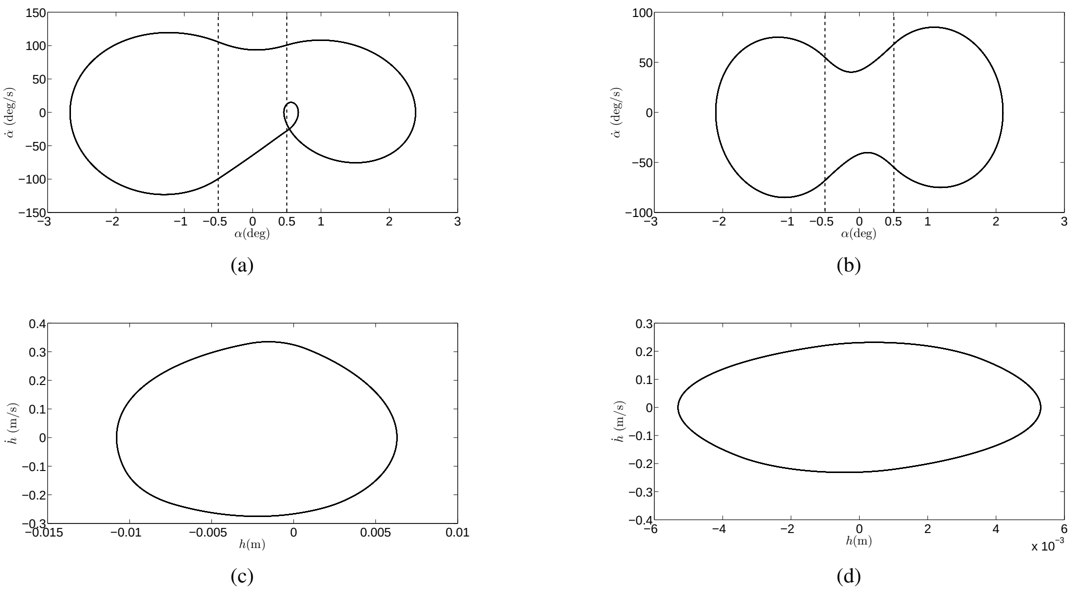

Figure 16: Phase portrait of the pitch and plunge motions (a,c) before the second transition $(34, 2m/s)$ and (b,d) after the second transition $(34, 4m/s)$.

the freeplay discontinuity boundary with a zero-pitch speed incidence, as shown in Figure 16(a). This phenomenon is due to the grazing bifurcation.

2. Phase space at second transition speed for different freeplay sizes

Near grazing and grazing phenomena is studied in this section. To this end, we investigate the transient phase portrait plots of the pitch motion at the second transition speed for both freeplay gaps, as shown in Figures 17(a) and 17(b). Clearly, we note that the transition or jump happens when the tangential motion between the small loop and the freeplay discontinuity boundary takes place. This result is true for both freeplay gap cases. It is noted that the tangential motion and the small loop disappear which make the pitch motion changes from period-doubling response to periodic response.

ISSN 2176-5480

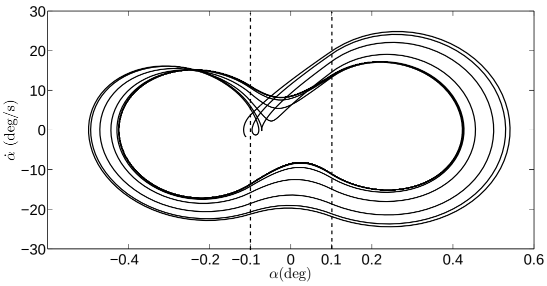

(a)

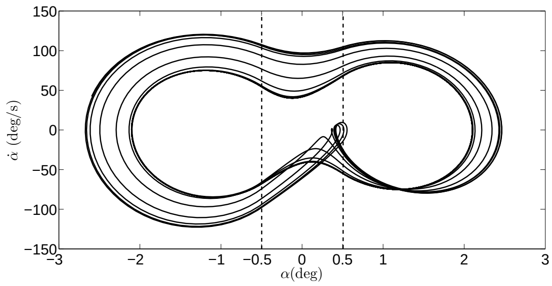

(b)

Figure 17: Phase portrait at transition speed for pitch motion: (a)freeplay of 0.1 degrees ($34.4m/s$), (b) freeplay of 0.5 degrees ($34.3m/s$)

CONCLUDING REMARKS

We investigated the effects of pitch freeplay nonlinearities on the behavior of a two degrees of freedom aeroelastic system. The freeplay nonlinearity was modeled based on the hyperbolic tangent representation. The unsteady formulation was used to model the aerodynamic loads. A linear analysis was performed to determine the coupled damping and frequencies and the associated linear flutter speed. A nonlinear analysis was also performed to investigate the effects of the freeplay size or gap on the behavior of the aeroelastic system. Two different gaps of pitch freeplay nonlinearity were considered to determine the effects of the size of the freeplay on the behavior of the aeroelastic and how the appearance of period-doubling responses are related to the grazing bifurcations. Two different transitions or sudden jumps were obtained when varying the freestream velocity (below linear flutter speed) for both freeplay nonlinearity gaps. These sudden transitions were caused by the tangential contact between the trajectory and the freeplay boundaries. These transitions were accompanied by a change in the response of the pitch motion from periodic to period-doubling in the first transition and from period-doubling to periodic in the second transition. These period-doubling events close to grazing impacts and at grazing bifurcation took place because of the presence of the freeplay nonlinearity.

ACKNOWLEDGEMENTS

The authors acknowledge the financial support of the São Paulo State Research Agency, FAPESP, Brazil (grant 2012/14273-6) and the Coordination for the Improvement of Higher Education Personnel (CAPES), Brazil (grant 0205109).

3. REFERENCES

Abdelkefi, A., Vasconcellos, R., Marques, F.D. and Hajj, M.R., 2012a. “Modeling and identification of freeplay nonlinearity”. *Journal of Sound and Vibration*, Vol. 331, pp. 1898–1907.

Abdelkefi, A., Vasconcellos, R., Nayfeh, A.H. and Hajj, M.R., 2012b. “An analytical and experimental investigation into limit-cycle oscillations of an aeroelastic system”. *Nonlinear Dynamics*, Vol. 71, pp. 159–173.

Balachandran, B., 2003. “Dynamics of an elastic structure excited by harmonic and aharmonic impactor motions”. *Journal of Vibration and Control*, Vol. 9, pp. 265–279.

Bisplinghoff, R.L., Ashley, H. and Halfman, R.L., 1996. *Aeroelasticity*. Dover.

Chakraborty, I. and Balachandran, B., 2012. “Near-grazing dynamics of base excited cantilevers with nonlinear tip interactions”. *Nonlinear Dynamics*, Vol. 70, pp. 1297–1310.

Chin, W., Ott, E., Nusse, H.E. and Grebogi, C., 1994. “Grazing bifurcations in impact oscillators”. *Physical Review E*, Vol. 50, pp. 4427–4444.

Conner, M.D., Tang, D.M., Dowell, E.H. and Virgin, L.N., 1996. “Nonlinear behavior of a typical airfoil section with control surface freeplay”. *Journal of Fluids and Structures*, , No. 11, pp. 89–109.

Dankowicz, H., Zhao, X. and Misra, S., 2007. “Near-grazing in tapping-mode atomic force microscopy”. *Int. J. Non-Linear Mechanics*, Vol. 42, pp. 697–709.

de Weger, J., Binks, D., Molenaar, J. and van de Water, W., 1996. “Generic behavior of gazing impact oscillators”. *Physical Review Letters*, Vol. 76, pp. 3951–3954.

di Bernardo, M., Champneys, A.R., Izhikevich, E.M., Bronner, B., Orbeck, N., Bao, J. and Shilnikov, A., 2006. “Two-parameter discontinuity-induced bifurcations of limit cycles: Classification and open problems”. *International Journal of Bifurcation and Chaos*, Vol. 16, pp. 601–629.

Dick, A.J., Balachandran, B., Yabuno, H., Numatsu, K., Hayashi, K., Kuroda, M. and Ashida, K., 2009. “Utilizing nonlinear phenomena to locate grazing in the constrained motion of a cantilever beam”. *Nonlinear Dynamics*, Vol. 57, pp. 335–349.

Edwards, J.W., Ashley, H. and Breakwell, J.V., 1979. "Unsteady aerodynamic modeling for arbitrary motions". *AIAA J.*, Vol. 17, pp. 365–374.

Fung, Y.C., 1993. *An introduction to the theory of Aeroelasticity*. New York: Dover Publications.

Henon, M., 1982. "On the numerical computation of poincaré maps". *Physica D*, , No. 5, pp. 412–414.

Jones, D.P., Roberts, I. and Gaitonde, A.L., 2007. "Identification of limit cycles for piecewise nonlinear". *Journal of Fluids and Structures*, Vol. 23, pp. 1012–1028.

Long, X.H., Lin, G. and Balachandran, B., 2008. "Grazing bifurcation in elastic structures excited by harmonic impactor motions". *Physica D*, Vol. 237, pp. 1129–1138.

Molenaar, J., de Weger, J.G. and va de Water, W., 2001. "Mappings of grazing impact oscillators". *Nonlinearity*, Vol. 14, pp. 301–321.

Moon, F.C. and Shaw, S.W., 1983. "Chaotic vibrations of a beam with non-linear boundary condidtions". *Int. J. Non-Linear Mechanics*, Vol. 18, pp. 465–477.

Nordmark, A.B., 1991. "Non-periodic motion caused by grazing incidence in an impact oscillator". *Journal of Sound and Vibration*, Vol. 145, pp. 279–297.

Roberts, I., Jones, D., Lieven, N., di Bernardo, M. and Champneys, A., 2002. "Analysis of piecewise linear aeroelastic systems using numerical continuation". In *Proceedings of the Institution of Mechanical Engineers*. Vol. 216, pp. 1 – 11.

Shaw, S.W., 1985. "Forced vibrations of a beam with one-sided amplitude constraint: Theory and experiment". *Journal of Sound and Vibration*, Vol. 99, pp. 199–212.

Shaw, S.W. and Holmes, P.J., 1983. "A periodically forced piecewise linear oscillator". *Journal of Sound and Vibration*, Vol. 90, pp. 129–155.

Stensson, A. and Nordmark, A.B., 1994. "Experimental investigation of some consequences of low velocity impacts in the chaotic dynamics of a mechanical system". *Philos. Trans. R. Soc. A*, Vol. 347, pp. 439–448.

Theodorsen, T., 1935. "General theory of aerodynamic instability and the mechanism of flutter". Technical Report 496, NACA.

Trickey, T., Virgin, L.N. and Dowell, H., 2002. "The stability of limit-cycle oscillations in an nonlinear aeroelastic system". *Proceedings: Mathematical, Physical and Engineering Sciences*, Vol. 458, No. 2025, pp. 2203–2226.

Vasconcellos, R., Abdelkefi, A., Marques, F.D. and Hajj, M.R., 2012. "Representation and analysis of control surface freeplay nonlinearity". *Journal of Fluids and Structures*, Vol. 31, pp. 79–91. doi:10.1016/j.jfluidstructs.2012.02.003.

Virgin, L.N. and Begley, C.G., 1999. "Grazing bifurcations and basins of attraction in an impact-friction". *Physica D*, Vol. 130, pp. 43–57.

Virgin, L.N., Dowell, E.H. and Conner, M.D., 1999. "On the evolution of deterministic non-periodic behavior of an airfoil". *Int. J. Nonlin. Mech.*, Vol. 34, pp. 499–514.

Whiston, G.S., 1987. "Global dynamics of a vibro-impacting linear oscillator". *Journal of Sound and Vibration*, Vol. 118, pp. 395–424.

4. RESPONSIBILITY NOTICE

The authors are the only responsible for the printed material included in this paper.